

Article

Influence of Gravitational Force on Particle Motion in the Channel Flow Induced by Fluid Injection

Konstantin Volkov

Institute of Hydrodynamics and Control Processes, St Petersburg State Marine Technical University,
190121 St Petersburg, Russia; k.volkov@kingston.ac.uk

Abstract: The motion of an individual particle in a circular channel flow induced with fluid injection is considered. Analysis takes into account drag and gravitational forces acting on an individual particle. The change in the radial structure of the flow in a channel with fluid injection on the motion of a particle is studied. A number of simplifying assumptions about the structure of the fluidflow in the channel makes it possible to obtain an analytical solution of the problem for particles. The results of a qualitative analysis of particle trajectories in the channel with fluid injection are compared with numerical simulations. The singular points of the particle trajectory are found in a wide range of characteristic non-dimensional parameters of the problem. The modes of motion of an individual particle in a channel with fluid injection are classified depending on the Stokes and Froude numbers.

Keywords: fluid injection; particle; trajectory; two-phase flow; channel; critical point



Citation: Volkov, K. Influence of Gravitational Force on Particle Motion in the Channel Flow Induced by Fluid Injection. *Fluids* **2022**, *7*, 328. <https://doi.org/10.3390/fluids7100328>

Academic Editors: Faik Hamad and Mehrdad Massoudi

Received: 8 September 2022

Accepted: 9 October 2022

Published: 14 October 2022

Publisher's Note: MDPI stays neutral with regard to jurisdictional claims in published maps and institutional affiliations.



Copyright: © 2022 by the authors. Licensee MDPI, Basel, Switzerland. This article is an open access article distributed under the terms and conditions of the Creative Commons Attribution (CC BY) license (<https://creativecommons.org/licenses/by/4.0/>).

1. Introduction

In the products of solid propellant combustion, along with the gas-phase component, there are solid and liquid combustion products of metal powders [1,2]. Simulation of two-phase flows of combustion products plays an important role in the study of intra-chamber processes in solid propellant rocket motors (SRM). The addition of solid particles to the flow complicates the flow pattern, which is associated with a variety of properties (inertia and concentration) of dispersed particles, which lead to the implementation of numerous flow regimes [3]. The concentration of particles is one of the main physical parameters that determine the characteristics of the movement of the dispersed phase, as well as the degree of its influence on the fluidflow [4]. In a dispersed medium, zones free of particles (fragmentation of the phase volume) and regions with intersecting particle trajectories can appear, at the boundaries of which the concentration of the dispersed phase increases sharply [5].

Analytical solutions of the Euler or Navier–Stokes equations contribute to a better understanding of the qualitative features of stationary and non-stationary flows. They allow estimating the domain of applicability of simplified mathematical models (inviscid fluid, slow flows, boundary layers) and are indispensable for validation of numerical and approximate methods. In the approaches developed in [6–8], self-similar solutions of the continuity equation and the momentum equations are found under the assumption of a linear dependence of the axial velocity on one of the spatial coordinates and uniform injection from the channel walls. An experimental validation of the analytical solution corresponding to the vortical flow of an inviscid incompressible fluid is carried out in [9–12], in which measurement data were obtained from the distributions of axial velocity and pressure at various Reynolds numbers.

The influence of compressibility increases at a sufficiently large distance from the inlet section of the channel, which leads to the filling of the axial velocity profile [12,13]. Turbulence has a rather weak effect on the structure of the mean flow, with the exception of the region adjacent to the outlet section of the channel, where there is a significant

acceleration of the flow, and the mean velocity profile becomes flatter [11]. The movement of the burning surface of the channel (the effect of non-stationarity of the process) has a comparatively weak effect on the velocity and pressure distributions [14]. The presence of a laminar flow region, which occupies the entire flow region (depending on the Reynolds number), is confirmed by [15,16].

To find a class of analytical solutions describing the flow of a viscous incompressible fluid in channels induced by fluid injection, methods of group analysis [17] are applied. The stability of the flow in a semi-infinite round pipe with a closed left end is considered in [18].

To take into account the influence of particles on the fluid flow, a joint calculation of the motion of the fluid and dispersed phases is required. Under certain restrictions on the particle size (the Stokes law for the particle drag) and the geometry of the computational domain (plane or axisymmetric channel), it is possible to construct analytical or approximate solutions that are convenient for making qualitative estimates and verifying numerical calculations. The mode of single particles is one of the simplest modes of particle-laden flow, which is realized at a low concentration of the dispersed phase. Obtaining new solutions is associated with the use of new dependencies describing the fluid flow and taking into account the influence of additional forces. Analytical or approximate solutions describing the motion of particles make it possible to find the limiting trajectory of particles (separatrix), to study the features of the concentration of the dispersed phase and their deposition on the wall [19,20].

Investigations of flows with particles in combustion chambers are related to the modeling of slagging of sections of the channel [21,22], combustion of aluminum particles [23,24], transport of particles by vortical structures and their interaction with an oscillating flow-field [25,26], and combustion instability [27,28]. The particle motion in channels with fluid injection and their influence on the characteristics of the carrier flow are studied in [29–32]. The motion of a particle in a propellant channel is considered in [33,34], in which an approach that simplifies the implementation of mathematical models of two-phase flows is proposed.

This study presents analytical solutions of equations describing the motion of an individual particle in a channel with fluid injection from walls, as well as the results of a numerical simulation of particle motion under the influence of non-turbulent factors. The influence of gravitational force on the motion of a particle is discussed and the domains of their applicability are investigated. The combustion surface is modeled by the injection surface of a mixture of fluid and particles, the parameters of which are known and do not depend on the place of injection and the presence of body forces.

2. Flow Induced by Fluid Injection

A flow in a circular channel, formed by injection of a mixture of fluid and dispersed particles with given parameters along the normal to the channel surface is considered. Flow is in a potential field of body forces, the vector of which is normal to the centerline of the channel. This model describes a gas-particle flow in a horizontal channel in the presence of gravity. It is assumed that the gravitational effects do not altered flowfield. The affect particle motion only.

A quasi-developed flow of a viscous incompressible fluid in a sufficiently long cylindrical channel with fluid injection is simulated, when the flow quantities, normalized on the velocity on the channel centerline, change slightly along its length. Fluid injection is uniformly distributed along cylindrical wall. The x axis is aligned with the centerline of the channel, and the y axis is normal to it (Figure 1). The radius of the channel is h , and the injection velocity v_w is the same at all points of the channel surface and directed along the normal to it. The spreading of the fluid occurs symmetrically with respect to plane $x = 0$ (mirror symmetry of the flow).

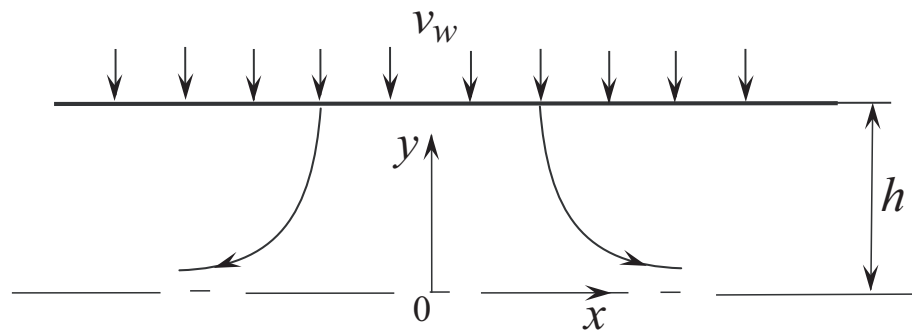


Figure 1. Flow induced by fluid injection.

The channel radius h is chosen as characteristic scale for variables with the dimension of length, and the injection velocity v_w is chosen as characteristic scale for variables with the dimension of velocity. The characteristic time is introduced as the ratio of the channel radius to the injection velocity, h/v_w . Potential body forces do not affect the fluid velocity in the channel [20], therefore the fluid velocity field is described by the relations that take place in the vortical flow of an inviscid incompressible fluid

$$\frac{u}{v_w} = \pi \frac{x}{h} \cos \left[\frac{\pi}{2} \left(\frac{r}{h} \right)^2 \right], \quad \frac{v}{v_w} = -\frac{h}{r} \sin \left[\frac{\pi}{2} \left(\frac{r}{h} \right)^2 \right]. \tag{1}$$

In this case, the influence of viscous effects manifests itself in rather narrow channels, while the influence of compressibility should be taken into account in long channels (Figure 2). The solid lines correspond to the results of numerical simulation [20], the dotted lines correspond to the vortical flow of an inviscid incompressible fluid, the symbols • correspond to experimental data. Profiles of axial velocity predicted with the developed model (solid lines) are flatter in the core region and steeper in the near wall region than those computed in vortical flow (dashed lines). The distributions of radial velocity computed with turbulence model and model of vortical flow are in a good agreement. Compressibility effects play an important role in a long channel leading to a flatter profile of axial velocity. Impact of Reynolds number on profiles of axial and radial velocities in flow induced by wall injection is small.

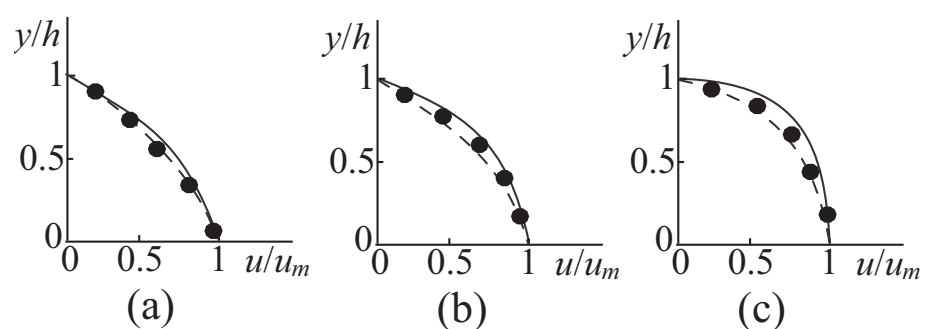


Figure 2. Axial velocity profiles in a channel for $x/h = 5$ (a); 15 (b); 30 (c). Solid lines correspond to the results of numerical simulation [20], dashed lines correspond to vortical flow described by Equation (1), and symbols *bullet* correspond to experimental data [8].

The influence of viscous effects on the flow structure in a channel with double-sided injection manifests itself mainly in the axial region, changing the fullness of the axial velocity profile (Figure 3). In a circular channel, as the injection intensity increases, the axial velocity profile becomes less filled and tends to a cosine profile (1) at $Re \rightarrow \infty$. The radial velocity profiles differ relatively little from each other in a wide range of injection

velocities. The maximum radial velocity is located at some distance from the channel wall and exceeds the injection velocity.

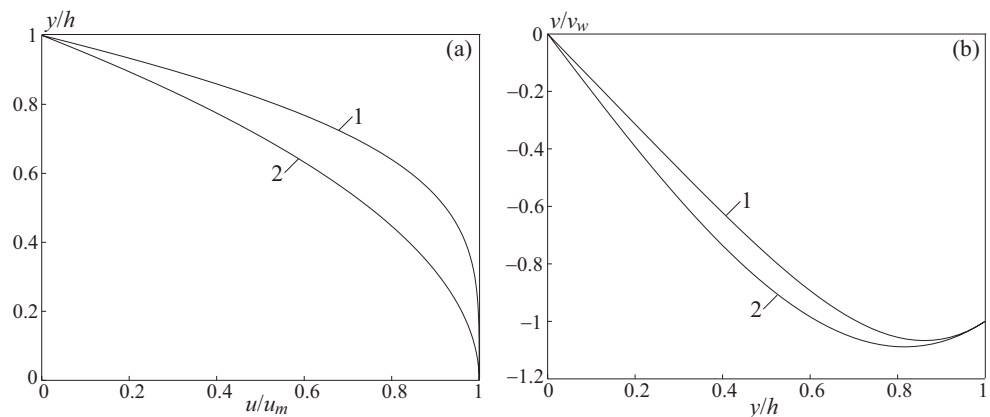


Figure 3. Profiles of axial velocity (a) and radial velocity (b) in a channel. Lines 1 and 2 correspond to the velocity profiles in channels with weak ($Re \rightarrow 0$) and strong ($Re \rightarrow \infty$) injection.

Particles are non-deformable spheres of the same diameter; their collisions and their effect on the fluid are neglected. In the model of interaction between a particle and a carrier flow, the drag force and gravity force are taken into account. The drag coefficient of a particle is found from the Stokes law.

The appearance of body forces complicates the problem, since the flow becomes three-dimensional. In this case, the flow parameters in the radial plane of the channel do not depend on the axial coordinate x (Figure 4).

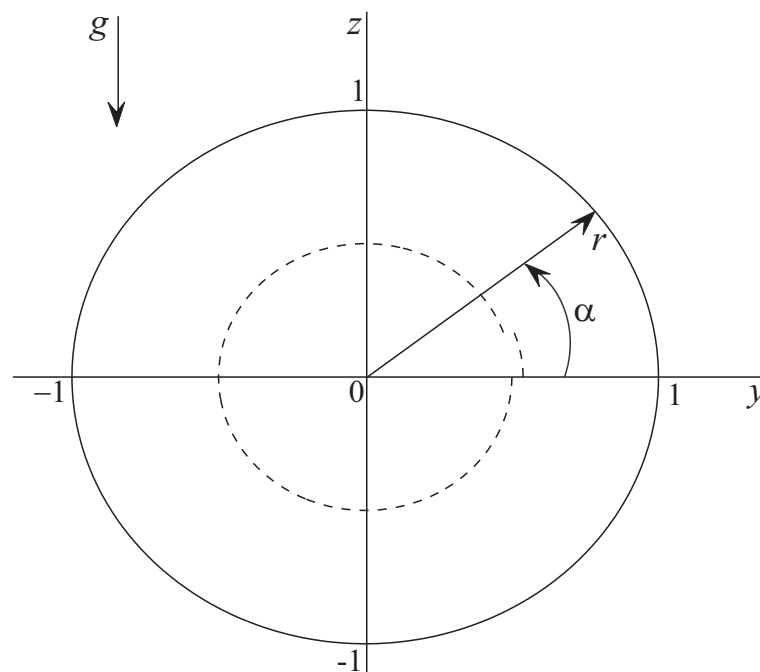


Figure 4. Frame of reference.

3. Governing Equations

In the discrete-trajectory approach, the equations describing the motion of a particle are written in Lagrangian variables and integrated along the trajectories of individual particles in a known (computed in advance) fluidfield.

The equation describing the translational motion of a spherical particle has the form

$$m_p \frac{dv_p}{dt} = \frac{1}{2} C_D \rho S_m (v - v_p)^2 + f_p, \tag{2}$$

where m_p is particle mass, S_m is particle midsection area, v and v_p are fluid velocity and particle velocity, respectively. The term f_p in Equation (2) includes forces of different nature, but different from the drag force, the account or disregard of which depends on the specific problem (for example, the gravity force is $f_p = m_p g$). The drag coefficient is represented as

$$C_D = \frac{24}{Re_p} f_D(Re_p).$$

The function f_D takes into account the correction for the inertia of the particle. The Reynolds number in the relative motion of a particle and fluid is found by the formula

$$Re_p = \frac{2r_p \rho |v - v_p|}{\mu},$$

where r_p is particle radius.

A kinematic relation is added to Equation (2), which makes it possible to calculate the radius vector of the particle's center of mass

$$\frac{dr_p}{dt} = v_p. \tag{3}$$

The temperature of a particle affects its motion through a correction to the drag coefficient. In many flow regimes, such a correction is small and is not taken into account.

Equations (2) and (3) are integrated along the particle trajectory and require the initial conditions (the coordinates and translational velocity of the particle at time $t = 0$). The fluid velocity is calculated at the points lying on the particle trajectory, $v = v(r_p)$.

4. Transformation of Coordinates

The motion of the particle is described in the Cartesian coordinate system. The equations describing the motion of a particle have the form

$$\frac{du_p}{dt} = \frac{s(r)x_p - u_p}{Stk}; \tag{4}$$

$$\frac{dv_p}{dt} = \frac{p(r)y_p - v_p}{Stk}; \tag{5}$$

$$\frac{dw_p}{dt} = \frac{p(r)z_p - w_p}{Stk} - Fr. \tag{6}$$

Here, $r^2 = y_p^2 + z_p^2$. The functions $s(r)$ and $p(r)$ in (1) are found from the relations

$$s(r) = \pi \cos\left(\frac{\pi}{2} r^2\right), \quad p(r) = -\frac{1}{r^2} \sin\left(\frac{\pi}{2} r^2\right).$$

Equations (4)–(6) are supplemented with kinematic relations that allow calculating the coordinates of the particle

$$\frac{dx_p}{dt} = u_p; \tag{7}$$

$$\frac{dy_p}{dt} = v_p; \tag{8}$$

$$\frac{dz_p}{dt} = w_p. \tag{9}$$

At the initial time $t = 0$ the particle is on the channel wall, therefore

$$x_{p0} = x_0, \quad y_{p0} = \cos \alpha, \quad z_{p0} = \sin \alpha.$$

The particle is injected from the wall along the normal to the surface, which gives

$$u_{p0} = 0, \quad v_{p0} = v_0 y_{p0}, \quad w_{p0} = v_0 z_{p0}.$$

Here, α and v_0 are the initial coordinate and initial velocity of the particle in the cylindrical coordinates (angle and velocity on the injection surface), and $\alpha \in [0, 2\pi]$ and $v_0 \in [0, 1]$.

The motion of a particle in a channel is determined by the Stokes and modified Froude numbers

$$\text{Stk} = \frac{\rho_p d_p^2 v_w}{18\mu h}, \quad \text{Fr} = \frac{hg}{v_w^2},$$

where g is gravitational acceleration.

5. Qualitative Analysis

The radial structure of a two-phase flow in a channel is determined by the system of Equations (4)–(9) and the corresponding initial conditions. Qualitative methods for the analysis of dynamical systems make it possible to systematize and generalize the solutions of the problem under various initial conditions and dimensionless parameters.

5.1. Zone of Gradient Flow

Near the channel centerline ($r \sim 0$, in practice for $r < 0.5$) functions are replaced by linear relations

$$s(r) = \pi, \quad p(r) = -\frac{\pi}{2}.$$

For small radii, the radial velocity gradient is equal to $-\pi/2$ and does not depend on the radial coordinate.

In the gradient flow zone, the system of Equations (4)–(9) becomes linear

$$\text{Stk} \frac{d^2 x_p}{dt^2} + \frac{dx_p}{dt} + \pi x_p = 0; \tag{10}$$

$$\text{Stk} \frac{d^2 y_p}{dt^2} + \frac{dy_p}{dt} + \frac{\pi}{2} y_p = 0; \tag{11}$$

$$\text{Stk} \frac{d^2 z_p}{dt^2} + \frac{dz_p}{dt} + \frac{\pi}{2} z_p + \text{Sf} = 0. \tag{12}$$

The parameter Sf is the product of the Stokes number and the Froude number ($\text{Sf} = \text{Re Fr}$).

Equations (10)–(12) are integrated independently of each other. A new variable is introduced

$$\widehat{z}_p = z_p + \frac{2}{\pi}Sf.$$

Then, Equations (11) and (12), describing the motion of a particle in the cross section of the channel, take the form

$$Stk \frac{d^2y_p}{dt^2} + \frac{dy_p}{dt} + \frac{\pi}{2}y_p = 0; \tag{13}$$

$$Stk \frac{d^2\widehat{z}_p}{dt^2} + \frac{d\widehat{z}_p}{dt} + \frac{\pi}{2}\widehat{z}_p = 0. \tag{14}$$

At the initial time $\widehat{z}_{p0} = z_{p0} + 2Sf/\pi$.

Equations (13) and (14) have the same form and are independent of each other. The introduction of a new variable makes it possible to eliminate the dependence on the Stokes and Froude numbers (parameter Sf). In the coordinate system (y_p, \widehat{z}_p) , the flow in the gradient zone is axisymmetric and does not depend on body forces.

The characteristic equation for Equations (13) and (14) has the form

$$Stk\lambda^2 + \lambda + \frac{\pi}{2} = 0.$$

Solving a quadratic equation, find its roots

$$\lambda_{1,2} = \frac{-1 \pm (1 - 2\pi Stk)^{1/2}}{2Stk}.$$

The roots of the characteristic equation show that there is a critical Stokes number $Stk_* = 1/2\pi$, which determines the change in qualitatively different two-phase flow regimes. For $Stk < Stk_*$, the particle does not cross the channel centerline (particle trajectories do not qualitatively differ from streamlines). For $Stk > Stk_*$ there is an intersection of the particle trajectory with the channel centerline.

The form of particle trajectories on the plane (y_p, \widehat{z}_p) with an arbitrary parameter Sf is obtained from the special case corresponding to $Sf = 0$. Particle trajectories are straight lines if the initial velocity vector of the particle at the boundary of the gradient zone is directed to a singular point located at the origin of the coordinate system (Figure 5), which requires that the condition

$$\frac{u_{p0}}{v_{p0}} = \frac{\widehat{z}_{p0}}{y_{p0}}.$$

Index 0 refers to the coordinates and initial velocity of the particle at the boundary of the gradient zone.

The particle trajectories obtained from the solution of Equations (13) and (14), under the specified condition and any Stokes number, are straight lines directed from the initial point on the injection surface to the singular point at the center of the channel. The oscillatory motion in the neighborhood of the singular point, which occurs at $Stk > Stk_*$, is along this straight line.

From a physical point of view, a singular point is a projection of the corresponding asymptote of the particle trajectories in the longitudinal section of the channel onto the radial plane. The singular point characterizes the limiting state of the particle at an unlimited time of its motion. The type of singular point depends on the Stokes number and its critical value.

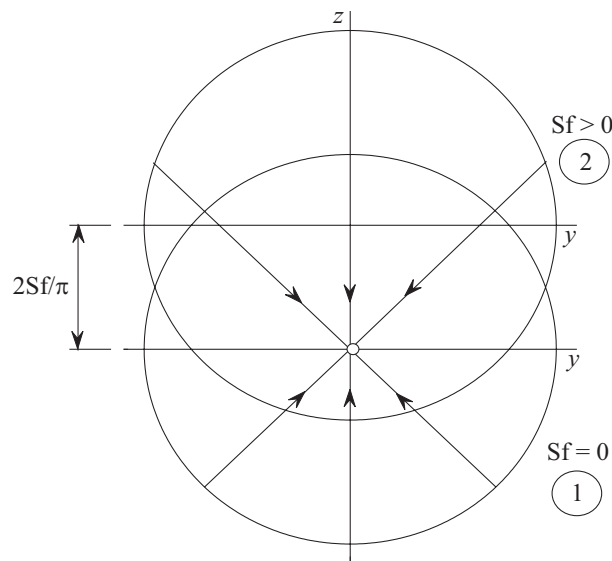


Figure 5. Particle trajectories in the gradient zone without (1) and with (2) of body forces.

At $Stk < Stk_*$ the particle trajectories monotonically approach the singular point (stable node). Particle trajectories are similar to streamlines. At $Stk > Stk_*$, an oscillatory regime (with damping) of particle motion along a straight line relative to a singular point (stable focus) is observed. Under these conditions, a specific flow zone is formed in the channel with its characteristic counter-oscillatory motion of particles. As the Stokes number increases, this zone expands. Since the concentration of particles in this zone increases, and the probability of their collision increases, to study the flow region with counter-oscillatory motion of particles, more advanced models are required, including, in particular, the effects of interaction of particles and coupling effects.

In the absence of body forces ($Sf = 0$), the singular point is at the center of the channel (the flow is axisymmetric). In the presence of body forces, the singular point is displaced in the direction of the vector of these forces. Approximately at $Sf < 0.7$, the singular point is in the region of the gradient fluid flow. The particle trajectories in the radial section of the channel, as in the case of $Sf = 0$, are still straight lines and are directed to a singular point, the type of which does not change within the gradient zone. The transition to the original coordinate system is graphically carried out by its shift along the z axis by $2Sf/\pi$ (Figure 5).

5.2. General Case

In the range $0.7 < Sf < 1$, Equations (4)–(9) describing particle motion are non-linear, which complicates their analysis and leads to the need to use numerical methods of analysis.

The gradient zone occupies the central, but smaller in terms of cross-sectional area, part of the channel. Outside this zone, the analysis is carried out on the basis of the original model described by Equations (10)–(12).

With the accepted direction of the gravity vector, the coordinates of singular points are found from the conditions

$$\alpha_* = -\frac{\pi}{2}, \quad \frac{1}{r_*} \sin\left(\frac{\pi}{2}r_*\right) = Sf.$$

Singular solution points exist only on the z axis in the lower part of the channel.

For small radii (for $r \rightarrow 0$), an approximate relation for the singular point coordinate is obtained, which is valid for the gradient flow zone

$$r_* = \frac{2}{\pi} Sf.$$

The dependence of the radial coordinate of the singular point r_* on the parameter Sf is shown in Figure 6. Line 1 corresponds to the numerical solution, and line 2 corresponds to an approximate relation valid for the gradient zone of the flow.

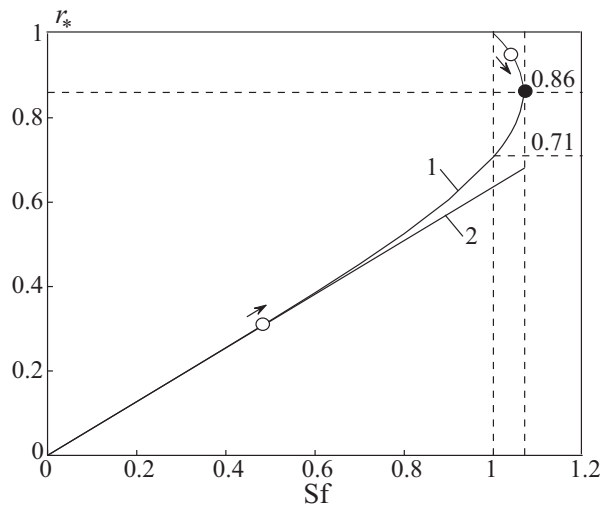


Figure 6. Dependence of the radial coordinate of a singular point on the Stokes and Froude numbers.

For $Sf = 0$, there is one singular point, which is located at the origin of the coordinate system. As Sf increases, the singular point moves along line 1 obtained by the numerical solution. For small r and Sf , line 1 is approximated with good accuracy by line 2. The position of the outer boundaries of the gradient zone is found at $r \approx 0.7$, which takes place at $Sf \approx 0.7$.

For $Sf = 1$, the second singular point appears at $r_* = 1$ (on the injection surface). As Sf increases further, the singular points approach each other (along line 1). For $Sf = 1.07$ and $r_* = 0.86$ these singular points merge and disappear. For $Sf > 1.07$, there are no singular points.

A connection between the presence and position of singular points on the phase plane and the kinematic structure of a two-phase flow in a channel is analyzed. On the phase plane, at the origin of the coordinate system (r_p, v_p) , there is a single singular point of the node type (particles do not cross the channel centerline) or focus (particles cross the channel centerline) depending on the Stokes number.

When body forces are taken into account, the singular point is displaced from the origin of the coordinate system down along the z axis. Changes in the structure of a two-phase flow in the longitudinal section of the channel are schematically shown in Figure 7 (at $Stk = 0.1$). For each Froude number, two trajectories of particles injected from the upper ($z = 1$) and lower ($z = -1$) surfaces of the channel are presented.

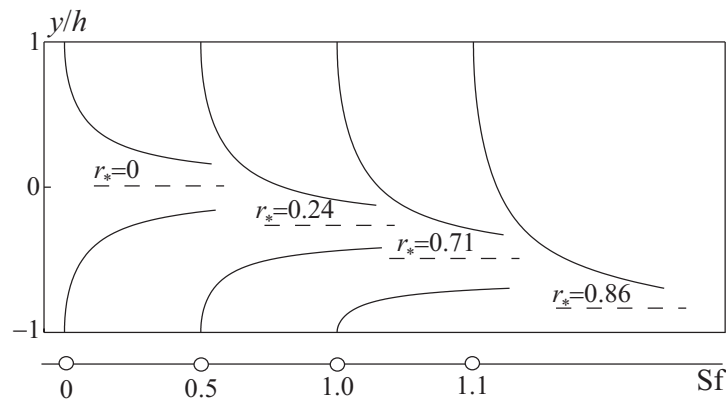


Figure 7. Change in the structure of two-phase flow in a channel with increasing Froude number.

As the Froude number increases, the asymptote of the axial (along the x axis) particle trajectories, defined as $z = r_*$, shifts downward. At $Sf = 1$ the second singular point appears (such as a saddle). This state characterizes a new quality of the system, when the drag force acting on the particle from the side of the fluid at the bottom of the channel are balanced by the mass force in opposite direction. This state is dynamically unstable, and with a slight increase in the initial velocity of the particles, they are carried away into the flow. At $Sf \approx 1.07$, which corresponds to the extreme value of the radial fluid velocity in the channel at $r_* \approx 0.86$, both singular points merge. In this case, the particles from the upper half of the channel reach the asymptote of the trajectories ($r_* \approx 0.86$), while the particles on its lower side are held by body forces. The zone free from particles of the corresponding size that appeared at $Sf = 1$ reaches its maximum size. For $Sf > 1.07$ there are no singular points. This leads to a new qualitative change in the flow regimes when the asymptote of the trajectories and the zone without particles disappear. Particles in the lower half of the channel cannot leave the blowing surface, and particles leaving the upper half of the channel also fall here (given sufficient time of motion). A further increase in the Stokes and Froude numbers (parameter Sf) does not cause qualitative changes in the flow.

6. Parameter Expansion Method

A modeling of two-phase flows in channels with fluid injection is analyzed with the parameter expansion method.

6.1. Velocity of Non-Equilibrium Motion

The motion of a Stokes particle of variable size, taking into account the body forces, is described by Equation (2), which is written in a dimensionless form

$$\frac{dv_p}{dt} = B(v_g - v_p) + Fr, \tag{15}$$

where $B = 1/(Stk \delta^2)$, $\delta = r_p/r_{p0}$. Index 0 refers to the start time.

The general solution of Equation (15), which is a linear ordinary differential equation of the 1st order, is presented as the sum of the general solution of the uniform equation and a partial solution of the non-uniform equation, $v_p = \hat{v}_p + \tilde{v}_p$. The general solution of the uniform equation has the form

$$\hat{v}_p = C_1 \exp(-F).$$

To find a partial solution of non-uniform equation, the method of expansion into a series in terms of the parameter is used

$$\tilde{v}_p = v_g + \sum_{k=1}^{\infty} (-1)^k Stk^k \frac{d^k v_g}{dt^k}.$$

Restricting the expansion to terms of the first order of smallness, the solution of Equation (15) takes the form

$$v_p = C_1 \exp(-F) + v_g + Stk(Fr - v_g t) \delta^2. \tag{16}$$

Here

$$F = \frac{1}{Stk} \int_0^t \frac{d\tau}{\delta^2(\tau)}, \quad C_1 = v_{p0} - v_g - Stk[Fr - (v_g t)_0].$$

The relation (16) shows that at $Stk \rightarrow 0$ the two-phase flow tends to equilibrium ($v_p \rightarrow v_g$). For $Stk \neq 0$ and $r_p \rightarrow 0$, flow reaches equilibrium state, $v_p \rightarrow v_g$. At the final

stage of evolution, the particles also come into a state of dynamic equilibrium with the fluid. For $\delta = 1$, a solution for a particle of constant size is obtained ($r_p = r_{p0}$).

The particle coordinates are found by resolving the kinematic relation

$$\frac{dr_p}{dt} = v_p. \tag{17}$$

Integration of Equation (17) over time from 0 to t , for $\delta \equiv 1$ gives

$$r_p = C_2 - C_1 \text{Stk} \exp(-t/\text{Stk}) + v_g t + \text{Stk}(\text{Fr} t - v_g). \tag{18}$$

Since the time in the relation (18) enters the term with the Stokes number as a factor, and the role of the exponential term decreases with decreasing Stokes number, the time of the equilibrium phase motion is used as the time.

The integration constants, C_1 and C_2 , are determined from the initial conditions. At time $t = 0$, the particle is on the channel wall, therefore

$$x_p(0) = x_{p0}, \quad y_p(0) = 1, \quad u_p(0) = 0, \quad v_p(0) = -\phi,$$

where ϕ is the parameter of the initial velocity non-equilibrium of the phases.

The obtained solution is linear with respect to the Stokes number and satisfactorily describes the particle trajectories in short channels. For $\text{Stk} \rightarrow \infty$ it qualitatively incorrectly reflects the behavior of the particle velocity.

Let us assume that at $t \leq t_b$, where t_b is the burning time of a particle, the change in particle size is described by the equation

$$r_p = r_{p0}(1 - t/t_b)^{1/q}.$$

For $q = 2$, which corresponds to the theoretical model of droplet combustion, the particle velocity is found from the relation

$$v_p = C(1 - Ft)^{1/(H\text{Stk})} + v_g + (1 - Ft)(\text{Fr} - v_g t)\text{Stk}.$$

The motion of a particle of variable size is determined by the parameter $H = t_p/t_b$, which is equal to the ratio of the time the particle stays in the channel $t_p = L/v_w$ and the burning time of the particle $t_b = d_{p0}^q/k$. The parameter characterizing the combustion of aluminum is represented as

$$H = \frac{kL}{v_w d_{p0}^q}.$$

As H increases, the conditions for particle combustion in the channel improve. For $H = \infty$ the particle burns on the channel surface, and for $H = 0$ the particle does not burn.

The Stokes number characterizes the velocity non-equilibrium of the phases. For $\text{Stk} \rightarrow 0$ the particle is completely entrained by the fluid, while for $\text{Stk} \rightarrow \infty$ its motion occurs independently of the fluid (for example, under the action of body forces). In the intermediate region, as the Stokes number increases, the velocity lag of the particle relative to the fluid increases.

At $\text{Stk} \rightarrow 0$, all parameters, excluding the combustion parameter H , become negligible, and a equilibrium two-phase flow with burning particles is characterized only by the parameter H .

6.2. Domain of Applicability of the Solution

The ratio (16) is transformed to the following form

$$|v_g - v_p| = C_1 \exp(-F) + \text{Stk}(\text{Fr} - v_g t)\delta^2. \tag{19}$$

The first term in the right side (19) determines the influence of the initial conditions, the second term is the mass forces, and the third term is the flow gradient. The criterion for the admissibility of the expansion of the particle velocity into a series in terms of the parameter is the condition for the smallness of the degree of velocity non-equilibrium of the phases

$$\left| \frac{v_g - v_p}{v_g} \right| \ll 1.$$

In this case, the smallness of the Stokes number is not required. For example, for a gradientless flow, the obtained relations are exact for any Stokes number.

The equilibrium conditions correspond to the case $C_1 \equiv 0$. There is no influence of the initial conditions on the further motion of the particle, and the equilibrium initial velocity is found from the relation

$$v_{p0} = v_g + [\text{Fr} - (v_g t)_0] \text{Stk}.$$

The intensity of attenuation of the influence of the initial state of the particle is determined by the Stokes number, and when a particle of variable mass moves, the influence of the initial conditions depends on its size.

Body forces affect the rate of non-equilibrium motion of phases through the Froude criterion. The influence of body forces increases with increasing Stokes number, decreases as δ decreases, and manifests itself to the greatest extent in low-velocity regions.

In a gradientless flow $dv_g/dt = 0$, and there is no influence of the gas-dynamic factor. For $dv_g/dt \neq 0$ the influence of the gas-dynamic factor increases as the Stokes number increases and decreases along with δ . The value of the derivative dv_g/dt depends on the geometric shape of the channel and reaches its maximum value in narrow channels and in places where the flow turns.

Taking the injection speed as the characteristic speed, and the ratio of the free volume of the combustion chamber to the fuel combustion area ($u = v_w, L = W/S$) as the characteristic size, the Stokes number is written as

$$\text{Stk} = \frac{\rho_p d_{p0}^2 v_w S}{18\mu W},$$

where W and S are volume and cross-sectional area of combustion chamber. When the propellant burns out, the parameter S/W decreases, which leads to a decrease in the degree of velocity non-equilibrium of the phases due to the weakening of the influence of the gas-dynamic factor.

6.3. Solution for Strong Injection

In channels with strong injection ($v_w \rightarrow \infty$), the relations (16) and (18) are presented in the analytical form. The particle coordinates are found from the relations

$$\begin{aligned} x &= x_0 \text{ch}^2(t/2), \\ y &= \frac{4}{\pi} \text{atan} \left[\exp \left(-\frac{\pi}{2} t \right) \right]. \end{aligned}$$

The time in the equilibrium motion of the phases is

$$t = \frac{-2}{\pi} \ln \left| \tan \left(\frac{\pi}{4} y \right) \right| = \frac{-1}{\pi} \ln \left| \frac{1 - \cos(\pi y/2)}{1 + \cos(\pi y/2)} \right|.$$

The constants of integration are found from the initial conditions

$$C_1 = \pi^2 \text{Stk} x_{p0}, \quad C_2 = 1 - \phi - \text{Stk}.$$

Up to the terms $O(\text{Stk}^2)$, the following relations, which give the velocities and coordinates of the particle at an arbitrary moment of time, are valid

$$\begin{aligned}
 u_p &= u_g + \frac{\pi^2}{4} \text{Stk} x_{p0} \exp(-t/\text{Stk}) - \frac{\pi^2}{4} \text{Stk} x_p; \\
 v_p &= v_g + (1 - \phi) \exp(-t/\text{Stk}) - \text{Stk} \left[\frac{\pi}{4} \sin(\pi y_p) \right]; \\
 x_p &= x - \frac{\pi}{2} \text{Stk} x \cos\left(\frac{\pi}{2} y\right); \\
 y_p &= y - \phi \text{Stk} - (1 - \phi) \text{Stk} \exp(-t/\text{Stk}) + \text{Stk} \sin\left(\frac{\pi}{2} y\right).
 \end{aligned}$$

The velocity distributions of the dispersed phase in the channel are shown in Figures 8 and 9 (results are normalized to the maximum velocity in the cross section, u_m , and injection velocity, v_w). Lines 1 correspond to the carrier flow, and lines 2–5 correspond to particles of various sizes. The influence of the initial non-equilibrium flow leads to deformation of the radial velocity profile of the dispersed phase near the injection surface. In general, the distributions of the radial velocity differ relatively little from each other in a wide range of problem parameters.

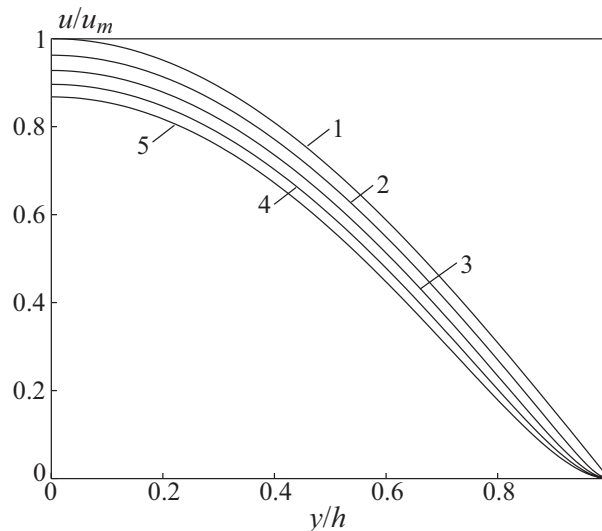


Figure 8. Distributions of axial velocity of particle for $\text{Stk} = 0.025$ (2); 0.05 (3); 0.075 (4); 0.1 (5). Line 1 correspond to fluidflow.

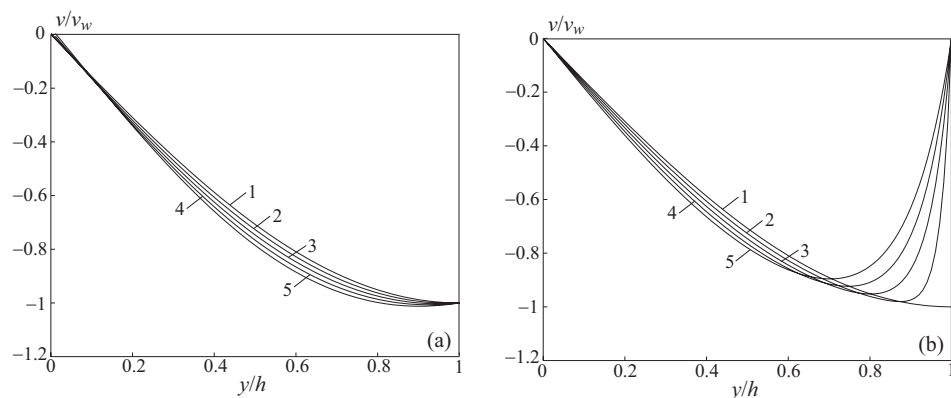


Figure 9. Distributions of radial velocity of particle for $\phi = 1$ (a) and $\phi = 0$ (b). Lines 2–5 correspond to different Stokes numbers $\text{Stk} = 0.025$ (2); 0.05 (3); 0.075 (4); 0.1 (5). Line 1 correspond to fluidflow.

7. Numerical Results

The results of numerical simulation are shown in Figures 10 and 11 for particles of different sizes. The Froude number is 1, and the Sf parameter is varied by appropriately changing the Stokes number. For each Stokes number, two trajectories for $z_{p0} = \pm 1$ (lower and upper walls of the channel) are given, and the position of the singular point (if it exists) is indicated. The prime corresponds to the particles injected from the bottom of the channel. The results are obtained at different initial particle velocity.

It follows from the calculations that for particles injected from the upper part of the channel, a change in the initial velocity has practically no effect on the shape of the phase trajectories (Figure 11a). Particles injected from the lower half of the channel turn out to be more sensitive to changes in the initial conditions (Figure 11b).

For $Sf = 0.1$, the singular point shifts slightly down along the z axis, and its type is a stable node. When Sf is increased to 0.5, the singular point type changes from node to focus. Accordingly, the type of phase trajectories also changes, which in the vicinity of the singular point acquire a damped oscillatory character. An increase in the initial particle velocity slightly affects the results.

For $Sf = 1$, the flow structure in the channel becomes more complicated. Due to the fact that the singular point is close enough to the lower surface of the channel, and the amplitude of particle oscillations near this point is significant, conditions arise for them to fall out of the flow. Particles located at the bottom of the channel at the initial moment at $v_{p0} = 0$ cannot leave the injection surface. However, an increase in the initial velocity module violates this dynamic equilibrium and leads to separation particles from the injection surface of the channel and their involvement in the flow, followed by asymptotic approximation to the corresponding singular point.

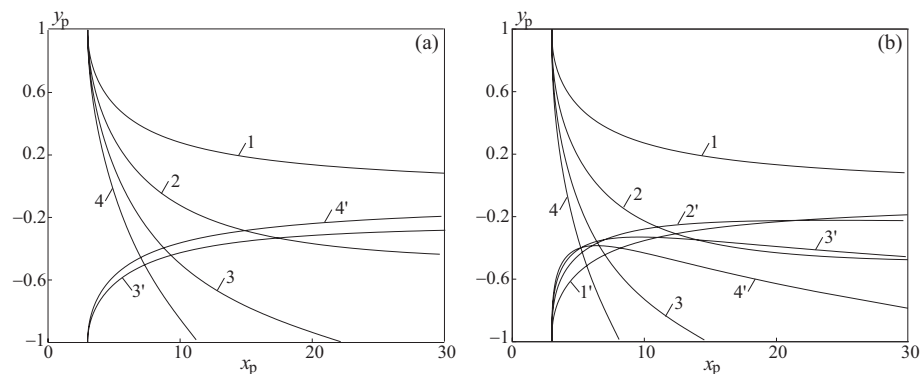


Figure 10. Trajectories of particle for $v_{p0} = 0$ (a) and $v_{p0} = 1$ (b) with different Stokes numbers $Stk = 0.1$ (1); 0.5 (2); 1.0 (3); 1.5 (4).

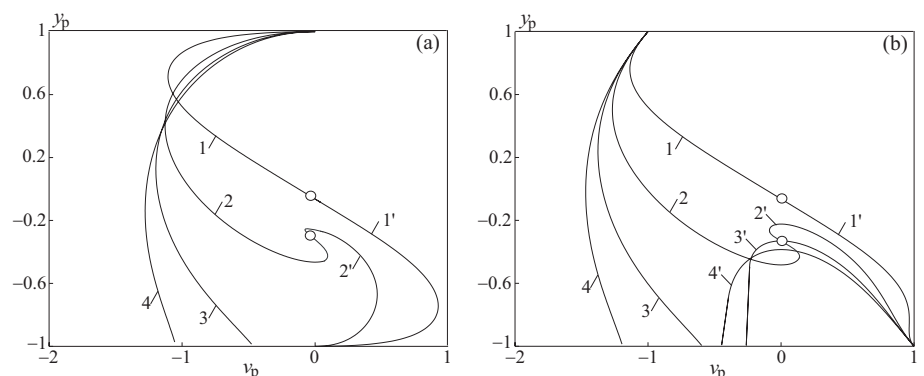


Figure 11. Solutions on phase plane (v_p, z_p) for $v_{p0} = 0$ (a) and $v_{p0} = 1$ (b) with different Stokes numbers $Stk = 0.1$ (1); 0.5 (2); 1.0 (3); 1.5 (4).

For $Sf = 1.5$ there are no singular points on the phase plane. Particles leaving the upper half of the channel eventually reach the lower surface, from which they cannot leave at zero initial velocity. An increase in the initial velocity of the particles leads to a temporary removal of particles from the lower part of the channel into the flow, followed by their fallout onto the same surface.

The trajectories of particles emerging from different points on the injection surface of the channel are shown in Figure 12 (for $Fr = 1$).

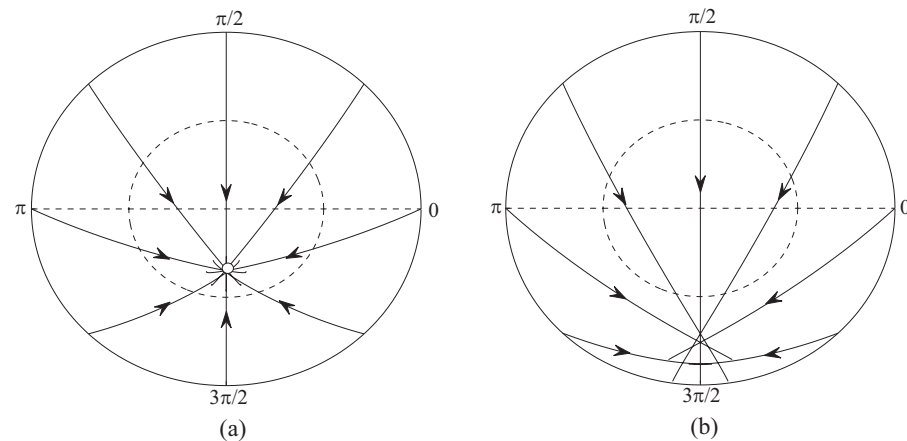


Figure 12. Trajectories of particles in cross section of channel for $Sf = 0.5$ (a) and $Sf = 1$ (b).

At $Sf = 0.5$, a specific zone of counter-oscillatory motion of particles is formed in the vicinity of the singular point. As the Sf parameter increases to 1, this zone expands, deforms, and captures the lower part of the channel. The change in the structure of this flow zone is accompanied by the precipitation of some particles from the flow onto the channel surface.

Depending on the Stokes number, the singular point is either a node or a focus. Outside the gradient zone, the critical Stokes number, which characterizes the change in the type of singular point, gradually increases as the singular point moves away from the center of the channel.

For $Sf = 1$, a second saddle-type singular point appears on the channel surface. The presence of two singular points, their relative proximity to each other and to the channel walls leads to the formation of a complex structure of a two-phase flow. New effects arise, in particular, the precipitation of particles from the flow onto the channel walls and the impossibility of their detachment from the injection surface. This is due to the fact that the oppositely directed drag and mass forces acting on the particles are approximately equal. As a consequence, under these conditions, the influence of secondary factors increases, for example, the initial velocity of particles on the injection surface.

8. Conclusions

A qualitative analysis of the trajectories of an individual particle in a channel with fluid injection from walls has been carried out. The computational domain is divided into a zone of gradient flow, in which the linearized equations of particle motion are applied, and a near-wall zone, in which an approximate solution of the problem is obtained. The results of the qualitative analysis are compared with numerical calculations, on the basis of which the singular points of the individual particle trajectory are found for various Stokes and Froude numbers.

The distributions of the dispersed phase parameters were obtained up to terms linear with respect to the Stokes number. Factors influencing the rate of non-equilibrium motion of phases are identified, and the domains of applicability of the obtained solution are investigated. The velocity and concentration distributions of particles in channels with strong injection are derived.

Funding: The research is partially funded by the Ministry of Science and Higher Education of the Russian Federation as part of World-class Research Center program: Advanced Digital Technologies (contract No. 075-15-2020-903 dated 16 November 2020).

Institutional Review Board Statement: Not applicable.

Informed Consent Statement: Not applicable.

Conflicts of Interest: The author declares no conflict of interest.

References

1. Emelyanov, V.N.; Teterina, I.V.; Volkov, K.N.; Garkushev, A.U. Pressure oscillations and instability of working processes in the combustion chambers of solid rocket motors. *Acta Astronaut.* **2017**, *135*, 161–171. [[CrossRef](#)]
2. Emelyanov, V.N.; Teterina, I.V.; Volkov, K.N. Dynamics and combustion of single aluminium agglomerate in solid propellant environment. *Acta Astronaut.* **2020**, *176*, 682–694. [[CrossRef](#)]
3. Volkov, K.N.; Emelyanov, V.N. *Flows of Gas with Particles*; Physical and Mathematical Publishing House: Moscow, Russia, 2008.
4. Varaksin, A.Y. *Turbulent Flows of Gas with Solid Particles*; Physical and Mathematical Publishing House: Moscow, Russia, 2003.
5. Osipov, A.N. Lagrangian modeling of dust admixture in gas flows. *Astrophys. Space Sci.* **2000**, *274*, 377–386. [[CrossRef](#)]
6. Berman, A.S. Laminar flow in channels with porous walls. *J. Appl. Phys.* **1953**, *24*, 1232–1235. [[CrossRef](#)]
7. Taylor, G.I. Fluid flow in regions bounded by porous surfaces. *Proc. R. Soc. Ser. A* **1956**, *234*, 456–475.
8. Culick, F.E.C. Rotational axisymmetric mean flow and damping of acoustic waves in a solid propellant rocket. *AIAA J.* **1966**, *4*, 1462–1464. [[CrossRef](#)]
9. Bundy, R.D.; Weissberg, H.L. Experimental study of fully developed laminar flow in a porous pipe with wall injection. *Phys. Fluids* **1970**, *13*, 2613–2615. [[CrossRef](#)]
10. Olson, R.M.; Eckert, E.R.G. Experimental studies of turbulent flow in a porous circular tube with uniform fluid injection through the tube wall. *J. Appl. Mech.* **1966**, *3*, 7–17. [[CrossRef](#)]
11. Yamada, K.; Ishikawa, N. Simulative study on the erosive burning of solid rocket motors pages. *AIAA J.* **1976**, *14*, 1170–1176. [[CrossRef](#)]
12. Dunlap, R.; Blackner, A.M.; Waugh, R.C.; Brown, R.S.; Willoughby, P.G. Internal flow field studies in a simulated cylindrical port rocket chamber. *J. Propuls. Power* **1990**, *6*, 690–704. [[CrossRef](#)]
13. Traineau, J.C.; Hervat, P.; Kuentzmann, P. Cold-flow simulation of a two-dimensional nozzleless solid-rocket motor. *AIAA Pap.* **1986**, 86-1447.
14. Majdalani, J.; Rienstra, S.W. Two forms of the rotational solution for wave propagation inside porous channels. *AIAA Pap.* **2022**, 2002-2985.
15. Apte, S.V.; Yang, V. Unsteady flow evolution in a porous chamber with surface mass injection, part 1: Free oscillations. *AIAA J.* **2001**, *39*, 1577–1586. [[CrossRef](#)]
16. Apte, S.V.; Yang, V. Unsteady flow evolution in a porous chamber with surface mass injection, part 2: Acoustic excitations. *AIAA J.* **2002**, *40*, 244–253. [[CrossRef](#)]
17. Boutros, Y.Z.; Abd-el-Malek, M.B.; Badran, N.A.; Hassan, H.S. Lie-group method for unsteady flows in a semi-infinite expanding or contracting pipe with injection or suction through a porous wall. *J. Comput. Appl. Math.* **2006**, *197*, 465–494. [[CrossRef](#)]
18. Griffond, J.; Casalis, G.; Pineau, J.-P. Spatial instability of flow in semiinfinite cylinder with fluid injection through its porous walls. *Eur. J. Mech. B/Fluids* **2000**, *19*, 69–87. [[CrossRef](#)]
19. Denisikhin, S.; Emelyanov, V.; Volkov, K. Fluid dynamics of thrust vectorable submerged nozzle. *Fluids* **2021**, *6*, 278. [[CrossRef](#)]
20. Emelyanov, V.N.; Volkov, K.N.; Yakovchuk, M.S. Multiparameter optimization of thrust vector control with transverse injection of a supersonic underexpanded gas jet into a convergent-divergent nozzle. *Energies* **2021**, *14*, 4359. [[CrossRef](#)]
21. Johnston, W.A.; Murdock, J.W.; Koshigoe, S.; Than P.T. Slag accumulation in the titan SRMU. *J. Propuls. Power* **1995**, *11*, 1012–1020. [[CrossRef](#)]
22. Salita, M. Defficiencies and requirements in modeling of slag generation in solid rocket motors. *J. Propuls. Power* **1995**, *11*, 10–23.
23. Cesco, N.; Dumas, L.; Peveigne, T.; Fabignon, Y. Stochastic models to the investigation of slag accumulation in a large solid rocket motors. *AIAA Pap.* **1997**, 97-2785.
24. Sabnis, J.S. Numerical simulation of distributed combustion in solid rocket motors with metallized propellants. *J. Propuls. Power* **2003**, *19*, 48–55. [[CrossRef](#)]
25. Dupays, J.; Prevost, M.; Tarrin, P.; Vuillot, F. Effects of particulate phase on vortex shedding driven oscillations in solid rocket motors. *AIAA Pap.* **1996**, 96-3248.
26. Vuillot, F.; Basset, T.; Dupays, J.; Daniel, E.; Lupoglazoff, N. 2D Navier–Stokes stability computations for solid rocket motors: Rotational, combustion, and two-phase flow effects. *AIAA Pap.* **1997**, 97-3326.
27. Cai, W.; Ma, F.; Yang, V. Two-phase vorticoacoustic flow interactions in solid-propellant rocket motors. *J. Propuls. Power* **2003**, *19*, 385–396. [[CrossRef](#)]
28. Daniel, E.; Thevand, N. Stability of acoustic wave in two-phase dilute flow with mass transfer. *AIAA J.* **2001**, *39*, 2121–2130. [[CrossRef](#)]

29. Majdalani, J.; van Moorhem, W.K. Laminar cold-flow model for the internal gas dynamics of a slab rocket motor. *Aerosp. Sci. Technol.* **2011**, *5*, 193–207. [[CrossRef](#)]
30. Feraille, T.; Casalis, G. Channel flow induced by wall injection of fluid and particles. *Phys. Fluids* **2003**, *15*, 348. [[CrossRef](#)]
31. Kabeel, A.; Elkelawy, M.; Bastawissi, H.; Elbanna, A. Solid particles injection in gas turbulent channel flow. *Energy Power Eng.* **2016**, *8*, 367–388. [[CrossRef](#)]
32. Al-Malki, M.; Hussain, Z.; Garrett, S.; Calabretto, S. Effects of parietal suction and injection on the stability of the Blasius boundary-layer flow over a permeable, heated plate. *Phys. Rev. Fluids* **2021**, *6*, 113902. [[CrossRef](#)]
33. Volkov, K.N. Motion of a condensed particle in a channel with injection. *J. Eng. Phys. Thermophys.* **2006**, *79*, 83–92. [[CrossRef](#)]
34. Volkov, K.N. Application of the parameter-expansion method to calculation of two-phase flows in channels with injection. *J. Eng. Phys. Thermophys.* **2006**, *79*, 1169–1178. [[CrossRef](#)]